NANO LETTERS

Letter

Cite This: Nano Lett. 2018, 18, 1442−1447

pubs.acs.org/NanoLett

Self-Assembled PCBM Nanosheets: A Facile Route to Electronic Layer-on-Layer Heterostructures

Hamid Reza Barzegar,[†,‡,§,∥] Christian Larsen,[‡] Nicolas Boulanger,[‡] Alex Zettl,[†,§,∥] Ludvig Edman,[*,‡] and Thomas Wågberg[*,‡]

[†]Department of Physics, University of California, Berkeley, California 94720, United States

[‡]Department of Physics, Umeå University, SE-901 87 Umeå, Sweden

[§]Materials Sciences Division, Lawrence Berkeley National Laboratory, Berkeley, California 94720, United States

[∥]Kavli Energy NanoSciences Institute at the University of California, Berkeley and the Lawrence Berkeley National Laboratory, Berkeley, California 94720, United States

Supporting Information

ABSTRACT: We report on the self-assembly of semicrystalline [6,6]-phenyl-C_{61}-butyric acid methyl ester (PCBM) nanosheets at the interface between a hydrophobic solvent and water, and utilize this opportunity for the realization of electronically active organic/organic molecular heterostructures. The self-assembled PCBM nanosheets can feature a lateral size of >1 cm^2 and be transferred from the water surface to both hydrophobic and hydrophilic surfaces using facile transfer techniques. We employ a transferred single PCBM nanosheet as the active material in a field-effect transistor (FET) and verify semiconductor function by a measured electron mobility of 1.2×10^{-2} cm^2 V^{-1} s^{-1} and an on−off ratio of ∼1×10^4. We further fabricate a planar organic/organic heterostructure with the p-type organic semiconductor poly(3-hexylthiophene-2,5-diyl) as the bottom layer and the n-type PCBM nanosheet as the top layer and demonstrate ambipolar FET operation with an electron mobility of 8.7×10^{-4} cm^2 V^{-1} s^{-1} and a hole mobility of 3.1×10^{-4} cm^2 V^{-1} s^{-1}.

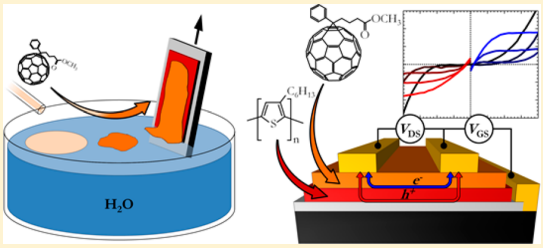

KEYWORDS: *Organic electronic, PCBM nanosheets, organic heterostructures, self-assembly*

The organic heterostructure in the form of a well-designed stack of thin layers of electronic molecular materials with specific function is a crucial building block in a plethora of emerging organic devices, including light-emitting diodes, ambipolar field-effect transistors (FETs), and solar cells.[1−8] The fabrication of well-defined planar heterostructures is however dependent on that the deposition of each layer does not damage the underlying stack, which is a requirement that is challenging to achieve with often preferred low-cost solution-based processes, as it commonly implies the employment of orthogonal solvent systems or sacrificial layers.[3,4,9−13] A few successful attempts at solution-based fabrication have been reported, including Langmuir−Blodgett, Langmuir−Schaefer, and liquid−liquid interfacial deposition,[14−17] but the vast majority of the current fabrication of planar organic heterostructures is executed using high-temperature vacuum deposition.[7,18,19] For some applications, this is a significant drawback, as vacuum-based fabrication is concomitant with a comparatively low throughput, poor material utilization, and high cost.[20]

Here, we report on the solution-based self-assembly of [6,6]-phenyl-C_{61}-butyric acid methyl ester (PCBM) molecules into planar and well-oriented 2D nanosheets at the interface between hydrophobic chloroform and water. We show that the PCBM nanosheets can be easily transferred to both hydrophilic and hydrophobic surfaces and that a transferred large-area nanosheet can feature a high electron mobility of 1.2×10^{-2} cm^2 V^{-1} s^{-1} in a FET device despite being fabricated in close contact with water under ambient-air atmosphere. We finally demonstrate the viability of the approach for the realization of planar organic heterostructures through the transfer of a hydrophobic PCBM nanosheet on top of a hydrophobic solution-processed poly(3-hexylthiophene-2,5-diyl) (P3HT) film. The solution-processed molecular heterostructure features ambipolar and balanced transport of electrons and holes, where the hole transport is provided for by the bottom P3HT while the electron transport is effectuated by the top PCBM layer. We accordingly introduce a novel solution-based method for the fabrication of organic heterostructures, where hydrophobic layers can be deposited directly on top of each other and where each layer performs a specific electronic function.

Figure 1a,b provides a schematic illustrating the synthesis of the PCBM nanosheets. A drop of a dilute PCBM-in-chloroform

Received: December 11, 2017
Revised: January 18, 2018
Published: January 24, 2018

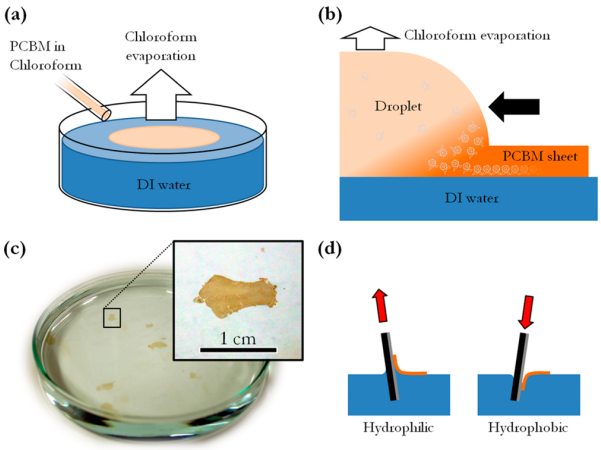

Figure 1. Schematic description of PCBM nanosheet fabrication. (a) Deposition of PCBM-in-chloroform solution in the form of a thin droplet on the surface of deionized water. (b) When the chloroform solvent evaporates (white arrow), the PCBM concentration in the droplet increases. Once the PCBM solution supersaturates, the PCBM molecules self-assemble into nanosheets at the edge of the shrinking (black arrow) droplet. (c) Photograph showing light-brown PCBM nanosheets floating on DI-water in a Petri dish. The inset shows a close-up of the highlighted PCBM sheet. (d) Schematic of methods to transfer PCBM nanosheets onto FET substrates with hydrophilic surface and hydrophobic surface. The PCBM nanosheets are deposited onto the hydrophilic substrates by withdrawing the substrate from the DI water, and on the hydrophobic substrates by submerging the substrate into the DI water.

solution is gently deposited onto the surface of deionized (DI) water positioned in a Petri dish. The solution spreads out and forms a thin surface layer on top of the DI water. As the chloroform evaporates away, the PCBM solution at the edges of the shrinking top layer becomes supersaturated at which point the PCBM molecules begin to self-assemble into a nanosheet (Figure 1b). The photograph in Figure 1c shows semi-transparent light-brown PCBM nanosheets floating on top of the DI water, following complete evaporation of the chloroform solvent. The inset in Figure 1c shows a close-up of a PCBM nanosheet, which reveals that the surface area of a typical nanosheet can be larger than 1 cm^2.

Figure 2a shows a high-resolution TEM image of a typical PCBM nanosheet, with the corresponding fast Fourier transform (FFT) displayed in the inset. The FFT comprises distinct spots and ring-shaped features, which are assigned to crystalline and amorphous regions, respectively. In other words, the PCBM nanosheet features a semicrystalline structure. The semicrystalline nanosheet structure is further confirmed by the selected area electron diffraction data presented in Figure S1. Figure 2b presents a higher-magnification TEM image of the area indicated by the dashed rectangle in Figure 2a, which visualizes PCBM molecules arranged in a crystalline hexagonal pattern (indicated by dashed hexagons) surrounded by amorphous PCBM regions. To establish the crystalline order, the bright spots of the FFT pattern were used for the reconstruction of the structure shown in Figure 2c. We find that this selected reconstructed structure indeed comprises PCBM molecules arranged in a hexagonal crystalline pattern.

We propose that the lower symmetry of the PCBM molecule in comparison to the fullerene C_{60} (that is due to the side chains) hinders a longer-range crystalline growth[21−23] and note that the semicrystalline PCBM nanosheet structure is similar to that reported for PCBM nanoribbons.[16] Moreover, due to the comparatively short nanosheet-growth time in the current study (typically less than a minute) this effect is more pronounced for the herein presented structures.

Water contact-angle measurements demonstrate that the bottom surface of the PCBM nanosheet is more hydrophilic than both its top surface and the top surface of an all-amorphous spin-coated PCBM film (see Table S1, for summary of results). These results thus suggest a preferential orientation of the as-synthesized nanosheets with their side-chains facing toward the water surface. We rationalize these findings with that the PCBM side-chains are more hydrophilic than the C_{60} core, partially because of the existence of electronegative oxygen atoms. Such a preferential orientation of PCBM molecules in the vicinity of a polar solvent has also been theoretically predicted.[16]

The PCBM nanosheets were measured to feature a mean thickness of 63 nm with a standard deviation of 23 nm, as derived from measurements on 62 different nanosheets. Considering the reported PCBM−PCBM intermolecular distance of 1.5 nm,[16,21] a nanosheet is composed of approximately 20 PCBM bilayers stacked on top of each other. We observe that PCBM nanosheets deposited on SiO_2/Si substrates display clear color variations from brown, over purple and blue, to green, when the nanosheet thickness increases from 22 to 115 nm.

In order to examine the electronic properties of the nanosheets, we employed a FET device architecture. Select

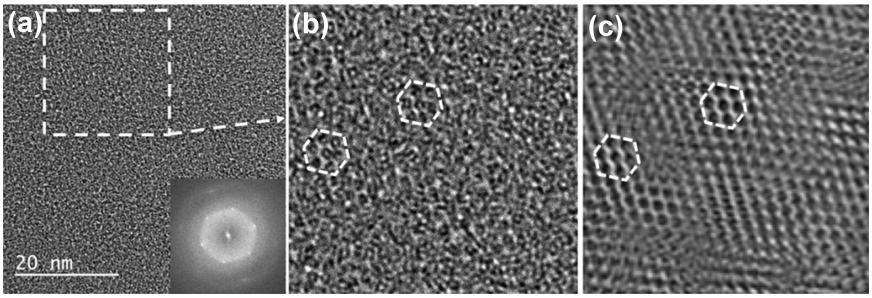

Figure 2. (a) High-resolution TEM image of a synthesized PCBM nanosheet. The inset presents the corresponding FFT with the combination of bright spots and the rings revealing a semicrystalline nanosheet structure. (b) Magnified TEM image of the area indicated by the dashed square in (a). The dashed hexagons indicate areas where the PCBM molecules are arranged in a crystalline hexagonal pattern. (c) Reconstructed image using solely the bright spots in the FFT pattern in the inset in (a). For comparison the same areas in (b,c) are highlighted by hexagons.

DOI: 10.1021/acs.nanolett.7b05205
Nano Lett. 2018, 18, 1442−1447

PCBM nanosheets were deposited onto p-Si/SiO_2 FET substrates by simply "fishing" them up from a clean DI water surface. Two distinctly different SiO_2 surfaces were prepared and evaluated: (i) a hydrophilic surface prepared by exposure to ultraviolet ozone (UVO) and (ii) a hydrophobic surface prepared by exposure to hexamethyldisilazane (HMDS) vapor.

The hydrophilic substrate was easily submerged into the DI water without disturbing the water surface. This allowed for a "fishing" of floating PCBM nanosheets from below, as shown in Figure 1d (left), thus forming a configuration where the bottom-layer of the PCBM nanosheet faces the hydrophilic SiO_2. The hydrophobic substrate instead displaces the DI water surface when immersed, which allows for a "dry" deposition, as depicted in Figure 1d (right). This results in a configuration with the top-layer of the PCBM nanosheet facing the hydrophobic SiO_2. All of the synthesis and transfer steps up to this point were performed under ambient-air atmosphere.

After deposition, the PCBM nanosheet on the p-Si/SiO_2 substrate was dried under vacuum, where after the source and drain Au electrodes were evaporated on top of the nanosheet to complete the FET fabrication. The transistor channel featured a width of W_D = 1 mm and a length of L_G = 50 μm, as defined by aligning a shadow-mask onto the PCBM nanosheet before the evaporation. A photograph of a complete FET device is shown in Figure S2 with the dashed red rectangle indicating a transistor channel fully covered by a PCBM nanosheet. We also prepared two sets of reference FETs by fabricating spin-coated PCBM FETs under identical conditions as the PCBM-nanosheet FETs and the recorded transistor data are summarized in Table S2.

The electrical characterization of the FETs was performed under a dry N_2 atmosphere. Figure 3a presents typical transfer curves for a hydrophobic (green squares) and a hydrophilic (blue circles) PCBM-nanosheet transistor. Average values for the I_{ON}/I_{OFF} ratio of ~10^4 and ~10^3 were recorded for the hydrophobic and hydrophilic devices, respectively. Typical output characteristics for a hydrophobic PCBM-nanosheet FET is shown in Figure 3b, and they reveal a linear increase of the drain-source current (I_{DS}) at low V_{DS} values and a well-behaved current saturation at high V_{DS} values.

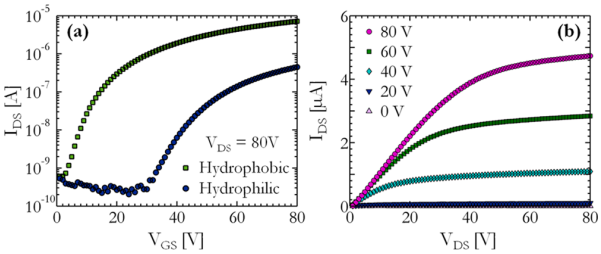

Figure 3. (a) The transfer characteristic of a typical hydrophobic (green squares) and hydrophilic (blue circles) PCBM-nanosheet FET. The inset displays the drain-source voltage (V_{DS}). (b) The output characteristics of a typical hydrophobic PCBM-nanosheet FET with the gate-source voltages (V_{GS}) presented in the inset.

The electron mobility (μ_e) and the threshold voltage (V_T) were extracted from the transfer measurements, following a procedure described in the experimental section. Only devices displaying a nanosheet coverage of the transistor channel of >90% were considered for the calculation of μ_e. (Note that the calculation of μ_e assumed a full channel coverage and that our procedure thus results in a slight underestimation of the true value for μ_e.) Table 1 presents the μ_e and V_T obtained from a total of 62 different PCBM nanosheet devices with the corresponding histogram distributions depicted in Figure S3.

The PCBM nanosheet on the hydrophobic substrate featured a higher μ_e and a lower V_T than the PCBM nanosheet on the hydrophilic substrate with the hero hydrophobic device featuring a high electron mobility of 1.2×10^{-2} cm^2 V^{-1} s^{-1}. The lower V_T of the PCBM nanosheet (and the spin-coated PCBM, see Table S2) on the hydrophobic substrate implies that the HMDS treatment successfully passivated the dangling bonds on the SiO_2 surface and effectively reduced the amount of trap-states at the interface.[24]

We mention that the high electron mobility was obtained on PCBM nanosheets synthesized under ambient air conditions and in close contact with water; previous studies on spin-coated PCBM films prepared under inert N_2 atmosphere have reported a mobility value in the same range (see Table S3).[4,25−32] This implies that the drying step successfully removed traces of water and solvent trapped within the nanosheet structure during fabrication.[33] It should further be noted that the presented molecular self-assembly method is ~20 times more material efficient than conventional spin-coating.

The synthesis of PCBM nanosheets on the surface of water allows for the realization of well-defined planar heterostructures, which would otherwise be difficult or impossible to achieve through sequential deposition from orthogonal solvent systems.[27,34] In this context, we do note that Morita et al. have successfully fabricated electronically active bilayer structures, comprising spin-coated PCBM and poly(3-hexylthiophene-2,5-diyl) (P3HT) nanosheets as the two distinct layers.[35]

Here, we begin by spin-coating a 15 nm thick film of P3HT on top of a Si/SiO_2 substrate. FETs based on solely the spin-coated P3HT film exhibits hole-only conduction characteristics, as shown in Figure S4 with a measured average hole mobility (μ_h) of 1.6×10^{-3} cm^2 V^{-1} s^{-1} (see Table 1). This spin-coated P3HT film comprises a highly hydrophobic surface, which facilitated for a "hydrophobic" transfer of the PCBM nanosheet

Table 1. Average Transistor Performance for the PCBM Nanosheet, the P3HT Thin Film, and the Bilayer P3HT/PCBM, with the Standard Deviation in Parentheses[a]

		electron		hole	
interface	no. of devices	μ_e [cm^2 V^{-1} s^{-1}]	V_T [V]	μ_h [cm^2 V^{-1} s^{-1}]	V_T [V]
hydrophilic/PCBM	37	**2.7×10^{-3}** $1.2(\pm0.6) \times 10^{-3}$	21(±14)	–	–
hydrophobic/PCBM	25	**1.2×10^{-2}** $5.8(\pm3.2) \times 10^{-3}$	15(±5)	–	–
pristine P3HT	22	–	–	**1.8×10^{-3}** $1.6(\pm0.1) \times 10^{-3}$	−18(±5)
ambipolar P3HT/PCBM	4	**8.7×10^{-4}** $5.1(\pm2.4) \times 10^{-4}$	13(±7)	**3.1×10^{-4}** $1.9(\pm0.8) \times 10^{-4}$	−7(±4)

[a]The hero-device mobility is presented in bold.

DOI: 10.1021/acs.nanolett.7b05205
Nano Lett. 2018, 18, 1442−1447

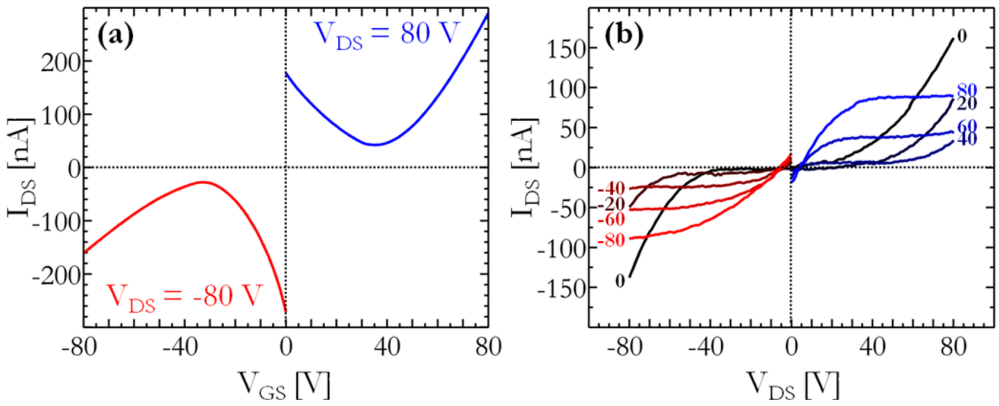

Figure 4. (a) The transfer and (b) output characteristics of an ambipolar P3HT/PCBM-nanosheet bilayer FET. The gate-source voltage is indicated at the corresponding current−voltage trace in (b).

with its top side facing the P3HT film (see Figure 1d, right). In this device structure, the bottom P3HT layer is expected to transport holes while the top PCBM nanosheet should transport the electrons. The bilayer FET architecture was finalized by evaporating Au drain and source electrodes on top of the P3HT/PCBM bilayer.

Figure 4a shows the transfer characteristics of a P3HT/PCBM-nanosheet bilayer FET, which demonstrates clear ambipolar behavior. Depending on the electrode bias, either electrons, holes, or both are conducted in the transistor channel. In the first quadrant (positive I_{DS} and V_{GS}), the increase in I_{DS} when $V_{GS} > 35$ V is due to improved electron transport through the PCBM nanosheet. In contrast, the increase in I_{DS} at $V_{GS} < 35$ V is due to improved hole transport through the P3HT layer. At $V_{GS} = 35$ V, the I_{DS} of 43 nA is carried by both electrons and holes and thus being ambipolar.[36] A similar behavior but with reversed charge and voltage polarity can be observed in the third quadrant (negative I_{DS} and V_{GS}). The values for μ_h and μ_e were calculated using the transfer data, and the data presented in Table 1 demonstrate a well-balanced ambipolar device. A similar balanced performance is observed in the output data in Figure 4b, where a well saturated and fairly symmetrical current behavior is obtained in both the first and third quadrants.

In conclusion, large-area and semicrystalline PCBM nanosheets are synthesized in a facile manner on a water surface. The synthesized nanosheets feature a high electron mobility of 1.2×10^{-2} cm^2 V^{-1} s^{-1}. The demonstrated facile transfer of the PCBM nanosheets onto various surfaces paves the way for the fabrication of planar heterostructures comprising PCBM and other 2D materials, as manifested in the demonstration of a functional ambipolar transistor comprising a PCBM nanosheet on top of a spin-coated P3HT film.

Methods. The PCBM nanosheets are synthesized at a DI water/chloroform interface. A solution of PCBM (>99.5%, Solenne BV) in chloroform (anhydrous, containing 0.5−1% ethanol stabilizer, Sigma-Aldrich) with concentration of 1 mg mL^{-1} is prepared and heated at 65 °C. Approximately 100 μL of the PCBM solution is gently placed at the surface of DI water (at room temperature) in a 5 cm wide beaker. The PCBM solution spreads on the surface of water and forms a floating thin droplet. As chloroform gradually evaporates the solution supersaturates and a thin PCBM nanosheet starts to form from at the edge of the droplet (as schematically shown in Figure 1a,b). We note that a small 0.5−1 vol % ethanol stabilizer, mixed into the chloroform, was found to aid in the formation of thinner droplets of the PCBM/chloroform solution on top of the DI-water, producing larger PCBM nanosheets. Chloroform typically comes with ethanol addition as a stabilizer (and can be used as is); however, synthesis of PCBM nanosheets with chloroform containing amylene stabilizer will benefit from the ethanol addition.

The desired PCBM nanosheets (with the right size and free of visible cracks and/or holes) are then transferred to a new beaker containing clean DI water; a clean glass slide is submerged in the water close to the desired PCBM nanosheets and is tilted so that it is located below the nanosheets. As the glass slide is pulled out of the beaker, the nanosheets stick to the surface of the glass slide. The glass slide, covered with the PCBM nanosheet, is then gently submerged in the fresh water in a new beaker until the PCBM nanosheet is released from the glass slide and floats on the surface of the water. For TEM measurements PCBM nanosheets were transferred to a lacey or quantifoil TEM grid and dried in ambient temperature. TEM imaging was performed using a JEOL 2010 (with LaB_6 gun) operated at 80 keV. The contact angle measurements were performed with an optical tensiometer (Attension Theta). The contact angle was recorded at 15 frames per second and was determined within 1 s of adding a 1−2 μL drop of DI water to the PCBM nanosheet surface in order to avoid evaporation effects.

Substrates of p-doped Si with a 200 nm thermally grown SiO_2 layer were used for the FET fabrication, and two different batches of substrates were used for device fabrication. The first batch was placed in a UV-ozone (UVO, model 42-220, Jelight Company Inc.) for 5 min in order to prepare a hydrophilic surface and the second batch was sequentially treated by a hexamethyldisilazane (HMDS, Sigma-Aldrich) vapor (in a beaker positioned on a hot-plate at 140 °C) for 5 min to prepare a hydrophobic surface. The PCBM nanosheets are then transferred to the UVO or HMDS treated FET substrate as described in the text and Figure 1d. We find that a wrinkle and crack free transfer of PCBM nanosheets (see inset in Figure S2) onto the hydrophobic (HMDS treated) surface was most successful when the substrate was submerged into the water with an angle of 65−75° with respect to the water surface. We note that not following such a process can lead to wrinkled PCBM sheets as observed on the TEM grid in Figure S5. For the pristine P3HT and the ambipolar devices, a 15 nm P3HT (regioregular, average M_n = 54,000−75,000 g mol^{-1}, Sigma-

DOI: 10.1021/acs.nanolett.7b05205
Nano Lett. 2018, 18, 1442−1447

Aldrich) film was first deposited onto the SiO_2 substrate by spin-coating from a 7 mg mL^{-1} solution in chlorobenzene (anhydrous, Sigma-Aldrich) followed by a 15 min annealing at 120 °C. The PCBM nanosheets were then sequentially deposited onto the P3HT surface by the method described above. All PCBM-nanosheet FETs were dried for 16 h at 100 °C in a vacuum oven before electrode evaporation of 50 nm Au source/drain electrodes. The Au was evaporated through a shadow-mask aligned to form FET channels with the deposited PCBM nanosheet. The channel dimensions, defined by the shadow mask, were L_G = 50 μm and a W_D = 1 mm. $I-V$ measurements on FETs were performed in a N_2 atmosphere ([O_2] < 1 ppm, [H_2O] < 1 ppm) using a semiconductor characterization system (SCS-4200, Keithley). The μ_e and V_T were obtained by fitting the measured transfer characteristics in the saturation regime to

$$\sqrt{I_{DS}} = \sqrt{\frac{\mu_e C_G W_D}{2L_G}}(V_{GS} - V_T) \quad (1)$$

where C_G is the gate capacitance.

The thickness of the PCBM nanosheets were measured on the FET devices after the $I-V$ characterization in close proximity to each measured channel using a stylus profilometer (DektakXT, Bruker).

■ ASSOCIATED CONTENT

Supporting Information

The Supporting Information is available free of charge on the ACS Publications website at DOI: 10.1021/acs.nanolett.7b05205.

TEM characterization of the nanosheets, results of contact angles measurements, statistic on device performance, photograph of device configuration, information on reference devices, and previous references (PDF)

■ AUTHOR INFORMATION

Corresponding Authors

*E-mail: Thomas.Wagberg@umu.se.

*E-mail: Ludivg.edman@umu.se.

ORCID

Hamid Reza Barzegar: 0000-0002-1314-5407

Christian Larsen: 0000-0002-2480-3786

Ludvig Edman: 0000-0003-2495-7037

Author Contributions

The manuscript was written through contributions of all authors. All authors have given approval to the final version of the manuscript. H.R.B. and C.L. contributed equally.

Notes

The authors declare no competing financial interest.

■ ACKNOWLEDGMENTS

This work was supported in part by the Swedish Research Council (Grant 2015-00520) which provided support for H.R.B. T.W. acknowledges support from Vetenskapsrådet (2017-04862) Energimyndigheten (45419-1), and Ångpanneföreningen (15-483). L.E. acknowledges financial support from the Swedish Foundation for Strategic Research, the Swedish Research Council and the Swedish Energy Agency. This work was supported in part by the Director, Office of Science, Office of Basic Energy Sciences, Materials Sciences and Engineering Division, of the U.S. Department of Energy under Contract No. DE-AC02-05-CH11231 within the sp2-Bonded Materials Program (KC2207), which provided for synthesis and TEM characterization.

■ REFERENCES

(1) Cho, S. W.; DeMasi, A.; Preston, A. R. H.; Smith, K. E.; Piper, L. F. J.; Chauhan, K. V.; Jones, T. S. *Appl. Phys. Lett.* **2012**, *100* (26), 263302.

(2) Ndjawa, G. O. N.; Graham, K. R.; Li, R. P.; Conron, S. M.; Erwin, P.; Chou, K. W.; Burkhard, G. F.; Zhao, K.; Hoke, E. T.; Thompson, M. E.; McGehee, M. D.; Amassian, A. *Chem. Mater.* **2015**, *27* (16), 5597−5604.

(3) Tada, A.; Geng, Y.; Wei, Q.; Hashimoto, K.; Tajima, K. *Nat. Mater.* **2011**, *10* (6), 450−455.

(4) Wei, Q.; Tajima, K.; Hashimoto, K. *ACS Appl. Mater. Interfaces* **2009**, *1* (9), 1865−1868.

(5) Stranks, S. D.; Yong, C. K.; Alexander-Webber, J. A.; Weisspfennig, C.; Johnston, M. B.; Herz, L. M.; Nicholas, R. J. *ACS Nano* **2012**, *6* (7), 6058−6066.

(6) Chang, J.-F.; Gwinner, M. C.; Caironi, M.; Sakanoue, T.; Sirringhaus, H. *Adv. Funct. Mater.* **2010**, *20* (17), 2825−2832.

(7) Dodabalapur, A.; Katz, H. E.; Torsi, L.; Haddon, R. C. *Science* **1995**, *269* (5230), 1560−1562.

(8) Zhang, M.; Hofle, S.; Czolk, J.; Mertens, A.; Colsmann, A. *Nanoscale* **2015**, *7* (47), 20009−20014.

(9) Wang, D. H.; Choi, D. G.; Lee, K. J.; Park, O. O.; Park, J. H. *Langmuir* **2010**, *26* (12), 9584−9588.

(10) Wang, D. H.; Choi, D. G.; Lee, K. J.; Im, S. H.; Park, O. O.; Park, J. H. *Org. Electron.* **2010**, *11* (8), 1376−1380.

(11) Nakamura, M.; Yang, C. H.; Zhou, E. J.; Tajima, K.; Hashimoto, K. *ACS Appl. Mater. Interfaces* **2009**, *1* (12), 2703−2706.

(12) Chen, L. C.; Degenaar, P.; Bradley, D. D. C. *Adv. Mater.* **2008**, *20* (9), 1679−1683.

(13) Cho, S.; Yuen, J.; Kim, J. Y.; Lee, K.; Heeger, A. J.; Lee, S. *Appl. Phys. Lett.* **2008**, *92* (6), 063505.

(14) Sizov, A. S.; Anisimov, D. S.; Agina, E. V.; Borshchev, O. V.; Bakirov, A. V.; Shcherbina, M. A.; Grigorian, S.; Bruevich, V. V.; Chvalun, S. N.; Paraschuk, D. Y.; Ponomarenko, S. A. *Langmuir* **2014**, *30* (50), 15327−15334.

(15) Nguyen, C. A.; Wang, J. L.; Chen, L.; Mhaisalkar, S. G.; Lee, P. S. *Org. Electron.* **2009**, *10* (1), 145−151.

(16) Gracia-Espino, E.; Barzegar, H. R.; Sharifi, T.; Yan, A.; Zettl, A.; Wågberg, T. *ACS Nano* **2015**, *9* (10), 10516−10522.

(17) Larsen, C.; Barzegar, H. R.; Nitze, F.; Wagberg, T.; Edman, L. *Nanotechnology* **2012**, *23* (34), 344015.

(18) Dinelli, F.; Capelli, R.; Loi, M. A.; Murgia, M.; Muccini, M.; Facchetti, A.; Marks, T. J. *Adv. Mater.* **2006**, *18* (11), 1416−1420.

(19) Rost, C.; Gundlach, D. J.; Karg, S.; Riess, W. *J. Appl. Phys.* **2004**, *95* (10), 5782−5787.

(20) Arias, A. C.; MacKenzie, J. D.; McCulloch, I.; Rivnay, J.; Salleo, A. *Chem. Rev.* **2010**, *110* (1), 3−24.

(21) Colle, R.; Grosso, G.; Ronzani, A.; Gazzano, M.; Palermo, V. *Carbon* **2012**, *50* (3), 1332−1337.

(22) Yang, Y.; Liu, C.; Gao, S.; Li, Y.; Wang, X. R.; Wang, Y.; Minari, T.; Xu, Y.; Wang, P.; Zhao, Y.; Tsukagoshi, K.; Shi, Y. *Mater. Chem. Phys.* **2014**, *145* (3), 327−333.

(23) Zheng, L.; Han, Y. *J. Phys. Chem. B* **2012**, *116* (5), 1598−1604.

(24) Chua, L.-L.; Zaumseil, J.; Chang, J.-F.; Ou, E. C. W.; Ho, P. K. H.; Sirringhaus, H.; Friend, R. H. *Nature* **2005**, *434* (7030), 194−199.

(25) Wang, J.; Larsen, C.; Wagberg, T.; Edman, L. *Adv. Funct. Mater.* **2011**, *21* (19), 3723−3728.

(26) Janasz, L.; Luczak, A.; Marszalek, T.; Dupont, B. G. R.; Jung, J.; Ulanski, J.; Pisula, W. *ACS Appl. Mater. Interfaces* **2017**, *9* (24), 20696−20703.

DOI: 10.1021/acs.nanolett.7b05205
Nano Lett. 2018, 18, 1442−1447

(27) Morana, M.; Koers, P.; Waldauf, C.; Koppe, M.; Muehlbacher, D.; Denk, P.; Scharber, M.; Waller, D.; Brabec, C. *Adv. Funct. Mater.* **2007**, *17* (16), 3274−3283.
(28) Rossbauer, S.; Müller, C.; Anthopoulos, T. D. *Adv. Funct. Mater.* **2014**, *24* (45), 7116−7124.
(29) Anthopoulos, T. D.; Tanase, C.; Setayesh, S.; Meijer, E. J.; Hummelen, J. C.; Blom, P. W. M.; de Leeuw, D. M. *Adv. Mater.* **2004**, *16* (23−24), 2174−2179.
(30) Chikamatsu, M.; Nagamatsu, S.; Yoshida, Y.; Saito, K.; Yase, K.; Kikuchi, K. *Appl. Phys. Lett.* **2005**, *87* (20), 203504.
(31) Morita, T.; Takashima, W.; Kaneto, K. *Jpn. J. Appl. Phys.* **2007**, *46* (11), L256.
(32) Seo, J. H.; Gutacker, A.; Walker, B.; Cho, S.; Garcia, A.; Yang, R.; Nguyen, T.-Q.; Heeger, A. J.; Bazan, G. C. *J. Am. Chem. Soc.* **2009**, *131* (51), 18220.
(33) Tapponnier, A.; Biaggio, I.; Günter, P. *Appl. Phys. Lett.* **2005**, *86* (11), 112114.
(34) Treat, N. D.; Brady, M. A.; Smith, G.; Toney, M. F.; Kramer, E. J.; Hawker, C. J.; Chabinyc, M. L. *Adv. Energy Mater.* **2011**, *1* (1), 82−89.
(35) Morita, T.; Singh, V.; Oku, S.; Nagamatsu, S.; Takashima, W.; Hayase, S.; Kaneto, K. *Jpn. J. Appl. Phys.* **2010**, *49* (4), 041601.
(36) Zaumseil, J.; Sirringhaus, H. *Chem. Rev.* **2007**, *107* (4), 1296−323.

DOI: 10.1021/acs.nanolett.7b05205
Nano Lett. 2018, 18, 1442−1447